ChemPubSoc Europe

DOI: 10.1002/chem.201701982

CHEMISTRY
A European Journal
Full Paper

Bimetallic Cooperativity

Bimetallic Cooperativity in Proton Reduction with an Amido-Bridged Cobalt Catalyst

Kenneth K. Kpogo[+],[a] Shivnath Mazumder[+],[a, c] Denan Wang,[b] H. Bernhard Schlegel,*[a] Adam T. Fiedler,*[b] and Cláudio N. Verani*[a]

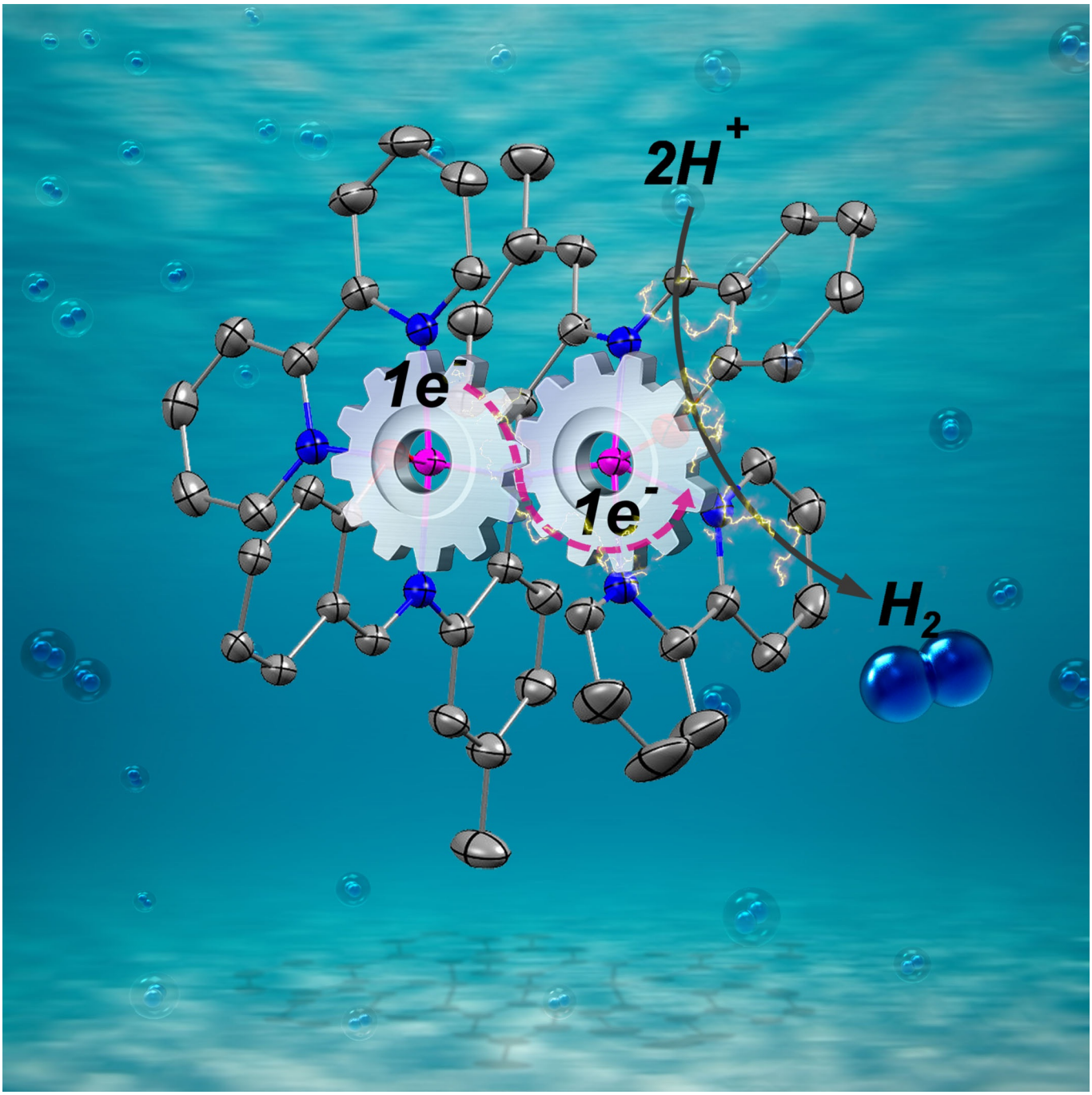

Abstract: The bimetallic catalyst $[Co^{II}_2(L^1)(bpy)_2]ClO_4$ (**1**), in which L^1 is an $[NN'_2O_2]$ fused ligand, efficiently reduced H^+ to H_2 in CH_3CN in the presence of 100 equiv of HOAc with a turnover number of 18 and a Faradaic efficiency of 94% after 3 h of bulk electrolysis at −1.6 V (vs. Ag/AgCl). This observation allowed the proposal that this bimetallic cooperativity is associated with distance, angle, and orbital alignment of the two Co centers, as promoted by the unique $Co–N_{amido}–Co$ environment offered by L^1. Experimental results revealed that the parent $[Co^{II}Co^{II}]$ complex undergoes two successive metal-based 1 e^- reductions to generate the catalytically active species $[Co^{I}Co^{I}]$, and DFT calculations suggested that addition of a proton to one Co^I triggers a cooperative 1 e^- transfer by each of these Co^I centers. This 2 e^- transfer is an alternative route to generate a more reactive $[Co^{II}(Co^{II}–H^-)]$ hydride, thus avoiding the $Co^{III}–H^-$ required in monometallic species. This $[Co^{II}(Co^{II}–H^-)]$ species then accepts another H^+ to release H_2.

Introduction

The widespread dependence of our society on fossil fuels and the impending depletion of carbon-based reserves have triggered the search for renewable and clean H-based energy.[1,2] Earth-abundant transition metals such as cobalt, nickel, and iron have attracted attention owing to their ability to generate H_2.[3–6] Among these metals, cobalt is particularly relevant because of its affordable redox potentials between the $3d^6$ Co^{III}, $3d^7$ Co^{II}, and $3d^8$ Co^I states. The catalytically active monovalent species can be stabilized and yield the doubly-oxidized cobalt/hydride intermediate $Co^{III}–H^-$, which is pivotal for H^+ reduction to H_2 after reduction to a more reactive $Co^{II}–H^-$.[7–11] Known cobalt catalysts follow either a heterolytic or a homolytic pathway.[9,12,13] The former mechanism relies on a single $Co^{III}–H^-$ or a $Co^{II}–H^-$[14,15] reacting with another H^+ and is favored if the concentration of protons is not limiting. The latter involves the collision of two $Co^{III}–H^-$ moieties from independent molecules.[16] Enhanced activity is expected from some binuclear analogues of monometallic catalysts in which close proximity between two Co centers triggers cooperativity either by facilitating homolytic pathways[17] or by enabling electron transfer between the metallic centers, thus avoiding formation of a $Co^{III}–H^-$ species.

Cooperative effects have been proposed by Dinolfo and co-workers[18] for a binuclear Co^{II} catalyst in a bicompartmental Robson/Okawa-type $[N_6O_2]$ macrocycle[19] with a Co–Co distance of 3.22 Å, whereas Gray and co-workers[20,21] evaluated oxime-based Co^{III} catalysts with both flexible hydrocarbon and rigid BO_4 bridges that revealed no significant catalytic enhancement. Similarly, the lack of cooperativity observed in dicobalt complexes featuring pyrazolato bridges[16,22] was attributed either to the large distance of 3.95 Å between the Co centers or to the flexibility of the ligand. To date it is unclear what factors control metal cooperativity in proton reduction, and this lack of understanding prevents a more rational design of Co_2 catalysts. Continuing our long-standing interest in the mechanisms of H_2 generation by Co catalysts,[23–26] we hypothesize that cooperativity will be dependent on 1) the distance between the Co centers, 2) the relative topology of the coordination environments, and 3) the degree of orientation and overlap between redox-active orbitals. To evaluate this hypothesis, we analyzed the catalytic potential of the bimetallic complex $[Co^{II}_2(L^1)(bpy)_2]ClO_4$ (**1**),[27] in which $(L^1)^{3-}$ is the triply deprotonated ligand shown in Figure 1a, by means of electrochemical, spectroscopic, and computational methods. Complex **1** is a unique bimetallic species singularly suited for this study because of the short distance between the two vicinal Co centers along with the presence of a $Co–N_{arylamido}–Co$ unit that may foster the proper orientation of Co orbitals involved in catalysis. Our results indicate that the two Co centers of complex **1** function cooperatively in the electrocatalytic reduction of H^+, thus offering a viable mechanistic alternative to homolytic and heterolytic pathways employed by mononuclear Co catalysts.

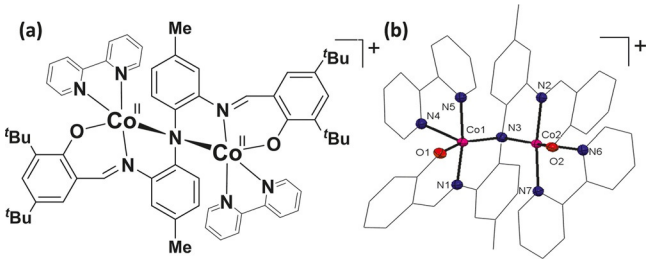

Figure 1. The complex $[Co^{II}_2(L^1)(bpy)_2]ClO_4$ (**1**): (a) Drawing and (b) Oak Ridge thermal ellipsoid plot (ORTEP) of the core showing a Co1–N3–Co2 angle of 86.9° expected to facilitate cooperativity.

[a] *K. K. Kpogo,[+] Dr. S. Mazumder,[+] Prof. H. B. Schlegel, Prof. C. N. Verani*
Department of Chemistry, Wayne State University
5101 Cass Ave, Detroit, MI 48202 (USA)
E-mail: hbs@chem.wayne.edu
cnverani@chem.wayne.edu

[b] *Dr. D. Wang, Prof. A. T. Fiedler*
Department of Chemistry, Marquette University
535 N. 14th St. Milwaukee, WI 53233 (USA)
E-mail: adam.fiedler@marquette.edu

[c] *Dr. S. Mazumder[+]*
Current address: Department of Chemistry, Hofstra University, Berliner Hall, Hempstead, NY 11549 (USA)

[+] *These authors contributed equally to this work.*

Supporting Information and the ORCID identification number(s) for the author(s) of this article can be found under https://doi.org/10.1002/chem.201701982.

Results and Discussion

Bimetallic $[Co^{II}_2(L^1)(bpy)_2]ClO_4$ (1)

Species **1** is prepared by treatment of 1 equiv of H_3L^1 with 2 equiv of $Co(ClO_4)_2{\cdot}6H_2O$ and bipyridine in the presence of Et_3N as base. A detailed description of the synthesis of **1**, along with its thorough characterization and molecular structure, was recently reported by Fiedler and co-workers.[27] Figure 1b shows that the $(L^1)^{3-}$ ligand loses two phenolic and one amidic protons to support a dicobalt(II) core in which the metal centers lie at a short distance of 2.70 Å, bridged by the N3 atom of a diarylamido unit with a Co1–N3–Co2 angle of 86.9°. Each of the five-coordinate Co^{II} centers is bonded to the N atom of an azomethine (N1 or N2) and the O atom of a phenolate (O1 or O2), with a bidentate bipyridine (bpy) completing the coordination sphere. This monocationic unit is neutralized by a single ClO_4^- counterion. The low-spin ($S=1/2$) nature of both Co^{II} centers is indicated by relatively short metal–ligand bond lengths, ranging between 1.89 and 2.06 Å (the average Co–N/O bond length is 1.95 Å). The Co^{II} centers are antiferromagnetically coupled as revealed by the sharpness of the ^1H NMR features.[27] The UV/Vis spectrum of **1** was recorded in CH_3CN (Figure 2). The catalyst presents a yellowish brown color owing to the presence of intense intraligand charge transfers (ILCTs). The initial spectrum shows bands below 320 nm tentatively attributed to $\sigma^*\leftarrow\sigma$ and $\pi^*\leftarrow\sigma$ ILCT processes, whereas the shoulders around 343 and 452 nm are attributed to low-intensity π–π^* transitions typical of distorted environments.[27]

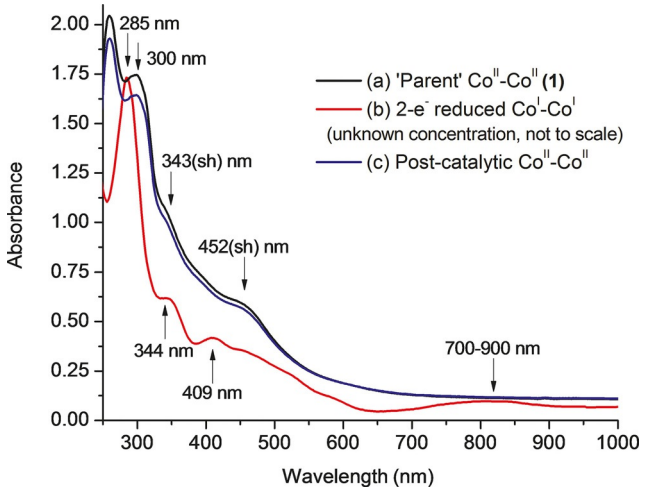

Figure 2. UV/Vis spectra of **1**: (a) Pre-catalytic $[Co^{II}Co^{II}]$ at 1×10^{-3} M; (b) chemically reduced $[Co^{I}Co^{I}]$, unknown concentration; (c) post-catalysis.

Electrocatalytic H^+ reduction

To study the possibility of **1** as a catalyst for the reduction of H^+ to H_2, we investigated the electrochemical response of **1** in anhydrous CH_3CN by using a glassy carbon working electrode with increasing concentrations of acetic acid (HOAc, $pK_a=22.3$ in CH_3CN) as the proton source.[28] The standard reduction potential of H^+ in CH_3CN, $E^{\circ(H^+/H_2)}$ was determined by open-circuit potential measurements as -0.028 ± 0.008 V (vs. Fc^+/Fc).[29] Under standard conditions, $E^{\circ(AH/A^-;H_2)}$ would be -1.35 V (vs. Fc^+/Fc) for HOAc; however, high concentrations can afford homoconjugation, leading to an incremental acidity and increasing the standard reduction potential.[29,30] As shown in Figure 3, a cyclic voltammogram of **1** shows three cathodic events. An irreversible wave was observed near -1.51 V (vs. Fc+/Fc) (-0.99 V vs. Ag/AgCl) and assigned to the reduction of the dicobalt(II) core $[Co^{II}Co^{II}]$ to the formal $[Co^{I}Co^{II}]$ state.

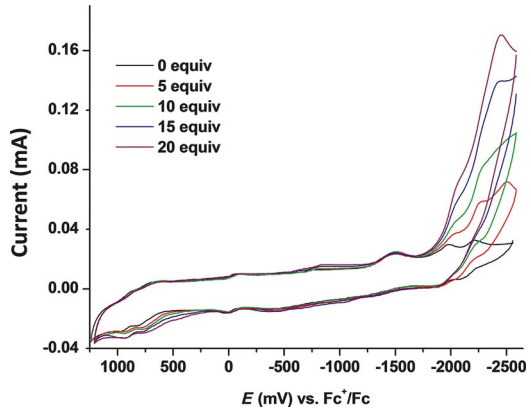

Figure 3. Cyclic voltammograms (CVs) of **1** (2.0 mM) measured vs. Ag/AgCl and plotted vs. Fc^+/Fc in the presence of increasing concentrations of HOAc. The CH_3CN solvent contained 0.1 M NBu_4PF_6 as the supporting electrolyte, and a glassy carbon working electrode was employed.

This $[Co^{I}Co^{II}]$ state does not seem able to afford catalysis, which is observed at a potential of -1.86 V (vs. Fc^+/Fc) (-1.34 V vs. Ag/AgCl), thus requiring a $[Co^{I}Co^{I}]$ state. Upon increase of the HOAc concentration, this electrocatalytic current enhancement becomes evident and reaches its maximum at -2.08 V (vs. Fc^+/Fc) (-1.56 V vs. Ag/AgCl) with the addition of 20 equiv of acid. Control experiments, in which HOAc is added to CH_3CN in absence of **1**, show negligible increase in current, even if significantly more negative potentials are applied. These results validate the catalytic role of **1** and support our hypothesis of homogeneous H^+ reduction with **1** as electrocatalyst.

The experimentally determined redox events were further studied by using DFT calculations in model compounds. Complex **1** was modeled with two low-spin Co^{II} centers in agreement with NMR data. Each center contains one unpaired electron, and the $[Co^{II}Co^{II}]$ core is antiferromagnetically coupled to provide a singlet ($S=0$) ground state.[27] For simplicity, the *t*Bu groups on the phenolates are replaced by methyl groups.[31] The results for relevant species are shown in Figure 4 as calculated spin-density plots with Mulliken spin-density values. The initial singlet $[Co^{II}Co^{II}]$ $^{LS}3d^7$–$^{LS}3d^7$ core in **1** is reduced to the doublet $[Co^{I}Co^{II}]$ $^{HS}3d^8$–$^{LS}3d^7$ core in **A**. Species **A**, therefore, contains a high-spin $3d^8$ Co^I with two unpaired electrons and can be further reduced to the singlet $[Co^{I}Co^{I}]$ **B** with a $^{HS}3d^8$–$^{HS}3d^8$ core at a calculated potential of -1.64 V (vs. Fc^+/Fc). The

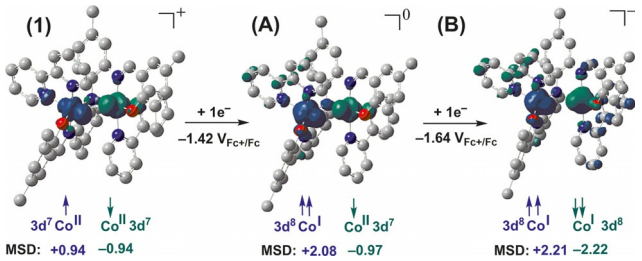

Figure 4. DFT-calculated spin-density plots (isodensity 0.004 a.u.), reduction potentials, and the Mulliken spin-density (MSD) values showing reduction of [$Co^{II}Co^{II}$] (**1**) to [$Co^{I}Co^{II}$] (**A**) to [$Co^{I}Co^{I}$] (**B**). H atoms are omitted for clarity.

presence of the monovalent species **B** was confirmed experimentally by UV/Vis spectroscopy by chemically reducing a sample of [$Co^{II}Co^{II}$] (**1**) with 2 equiv of KC_8 under inert atmosphere. The resulting spectrum is shown in Figure 2b and displays bands typical of previously reported Co^{I} species; based on similarities to the spectrum of the Co^{II}-containing species, the band at 285 nm is attributed to ILCT processes. Bands at 344, 409, and 700–900 nm are comparable to those observed for a Co^{I} tetraaza-macrocyclic catalyst[32] and associated with d–d bands. In an octahedral Co^{I} bis(pyridine-2,6-diimine) complex these broad bands are attributed to d–π* charge-transfer processes,[33] whereas several shoulders at 500–600 nm are characteristic for the presence of radical species. Similar shoulders were observed for **B** between 450 and 650 nm, thus suggesting that ligand reduction may have occurred to some extent. To ascertain experimentally the overpotential at which **1** shows electrocatalytic activity, a series of 2 min bulk electrolyses (BE) were performed at applied potentials ranging between −0.7 and −1.6 V (vs. Ag/AgCl). The experiment was performed in an airtight H-type cell by using a Hg-pool working electrode, Ag/AgCl as reference, and a Pt-coil auxiliary electrode placed in an adjacent compartment separated by a frit. The main chamber was filled with catalyst **1**, $TBAPF_6$ (TBA = tetrabutylammonium) electrolyte solution, and HOAc in 20 mL CH_3CN. The auxiliary chamber was filled with the electrolyte solution only. Figure 5a illustrates the total charge consumed by **1** in the presence of acid during BE; charge consumption remained constant up to −1.4 V (vs. Ag/AgCl), after which it increased significantly until −1.6 V (vs. Ag/AgCl), concomitant with evolution of H_2 gas, as confirmed by GC. Figure 5b shows a plot of charge consumed versus applied potential. The graph

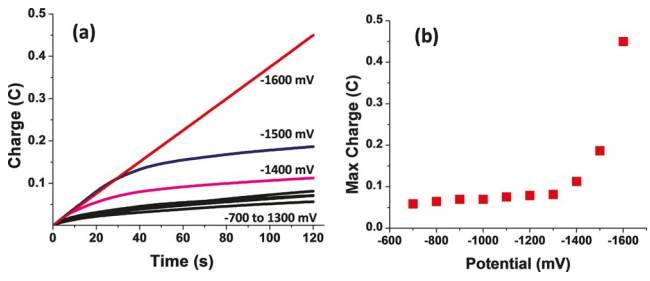

Figure 5. (a) Charge consumed at variable potentials (vs. Ag/AgCl) with 2 min. BE; (b) maximum charge consumed vs. potential (vs. Ag/AgCl).

indicates that the onset potential for catalysis is −1.4 V (vs. Ag/AgCl).

This onset potential is comparable to that of the mononuclear cobalt polypyridyl catalyst recently published by Verani and co-workers[24] and investigated under similar conditions that enable comparison. The plot of current versus concentration of HOAc at a potential of −2.08 V (vs. Fc^{+}/Fc) is provided in Figure 6. The measured current increases linearly with the

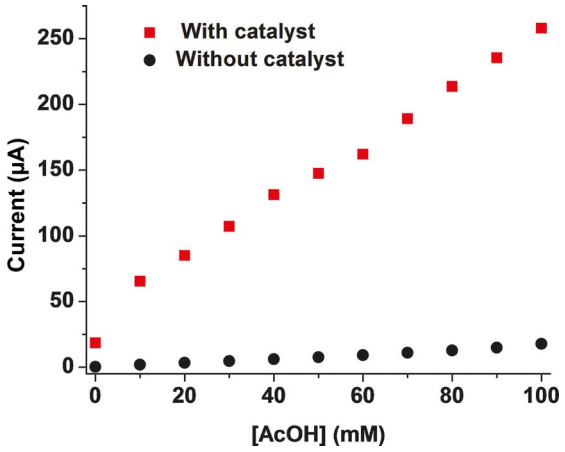

Figure 6. Squares: CV current at −2.08 V (vs. Fc^{+}/Fc) as a function of HOAc concentration for solutions of **1** (2.0 mM) in CH_3CN; circles: corresponding data measured under identical conditions but in the absence of **1**.

concentration of HOAc, whereas negligible current increase is observed in absence of **1**. An apparent overpotential of 0.63 V was calculated assuming homoconjugation ($E_{Fc^{+}/Fc}$ AcOH in CH_3CN = −1.23 V), and a rate of H_2 generation[30] (k_{obs}) of 6.33 s^{-1} resulted. A charge consumption plot over 3 h is shown in Figure 7. The slight curvature observed within the first 10 min is typical for proton reduction and tentatively associated with solvent dissociation.[25] The amount of H_2 produced over the same period of time was determined by BE as already

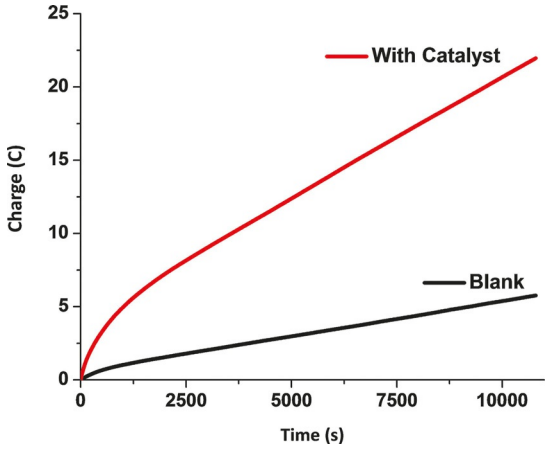

Figure 7. Charge consumption versus time during BE with $TBAPF_6$ (1.560 g), HOAc (0.024 g, 0.4 mmol), **1** (0.0047 g, 0.004 mmol), and CH_3CN (20 mL) at −1.6 V (vs. Ag/AgCl).

discussed, by using 100 equiv of acid at an applied potential of −1.6 V (vs. Ag/AgCl).

A sample of the headspace gas (100 μL) was injected into a GC to quantify the amount of H_2 produced and repeated in triplicate. A calibration curve (Figure S1 in the Supporting Information) was used to standardize the calculations. An average amount of 0.072 mmol H_2 was calculated after background correction, which is associated with a turnover number (TON) of 18, equivalent to approximately 40% conversion rate. The Faradaic efficiency (FE) was calculated at 94% from the maximum charge consumed. BE experiments were performed under similar conditions as described above by using an incremental concentration of acid, leading to an increase in the calculated TONs. Accordingly, the use of 200 equiv of acid led to a TON of 75, whereas 300 equiv led to a TON of 97. In both cases the Faradaic efficiency remained consistent at >90%. As expected, because the concentration of acid was no longer a limiting factor, high yields were observed and the use of 400 equiv of acid led to the highest TON of 120 with an associated drop in FE to approximately 85%.

The charge versus time plots for these experiments are shown in Figures S2–S4 in the Supporting Information; whereas the first two graphs show an almost linear behavior in which the initial lagging observed in Figure 6 almost disappears, the plot with 400 equiv shows slightly increased activity after the first 10 min followed by a decrease after approximately 2.5 h, which is likely related to slow degradation of the catalyst under such acidic conditions. Considering the near-linearity of the graph in Figure S3, the system seems optimized in the presence of 200 equiv of acid. Comparison of activity with other reported bimetallic species[16,18,20,34] is hampered by the lack of information on directly measured TONs. However, simple assessment of our system (without considering variables such as proton source and applied potential) reveals that the TON, rate of conversion, and Faradaic efficiency values compare favorably with monocobalt catalysts.[23,24]

Fate of catalyst 1

The post-catalysis spectrum shown in Figure 2c displays features similar to those observed in the [$Co^{II}Co^{II}$] state (Figure 2a), thus attesting to the catalytic nature of **1** along with a decrease of approximately 10% in the UV bands and of 2% in the 450 nm band. This small discrepancy is explained by slow percolation of the solution between the chambers and through the frit of the electrochemical cell. Alternatively, a fraction of the catalyst may be deactivated, and evaluation of a grafoil sheet electrode was performed by scanning electron microscopy (SEM) and energy-dispersive X-ray (EDX) analysis to assess the possibility of nanoparticle formation (Figure S5 in the Supporting Information). Notwithstanding evidence for formation of organic nanoparticles, no Co was detected on the surface of the electrode. Thus, UV/Vis, SEM, and EDX analyses support the presence of a catalyst that is molecular in nature.

Mechanism of H^+ reduction

The proposed catalytic mechanism of H^+ reduction is shown in Figure 8. Each $^{LS}3d^7$ ion in [$Co^{II}Co^{II}$] (**1**) displays one unpaired electron in the d_{z^2}-based singly occupied molecular orbital (SOMO), yielding an antiferromagnetically coupled singlet ($S=0$). The reduction of **1** generates [$Co^{I}Co^{II}$] (**A**) with a Co^{I} ($^{HS}3d^8$) and a Co^{II} ($^{LS}3d^7$). The Co^{I}-based $d_{x^2-y^2}$ orbital is now occupied by an electron, leading to an overall doublet ($S=1/2$) ground state. On further reduction the second Co^{II} center in **A** accepts

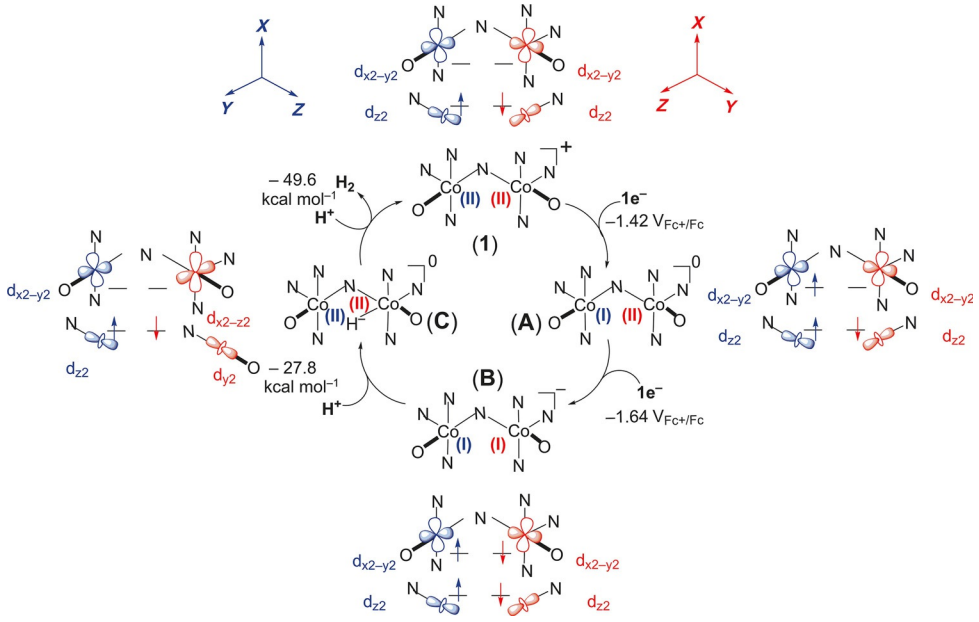

Figure 8. Catalytic mechanism of H_2 generation by **1** in CH_3CN. Protonation of the [$Co^{I}Co^{I}$] intermediate **B** causes each Co^{I} center to donate 1 e^- to H^+, resulting in the formation of the [$Co^{II}Co^{II}$]-hydride complex **C**. Isodensity plots of the orbitals of **1**, **A**, **B**, and **C** are shown in Figure S7 in the Supporting Information. Free energies [kcal mol^{-1}][35] and potentials [V] calculated at the BPW91/SDD/6-31G(d,p) level of theory.[36]

an electron to its empty $d_{x^2-y^2}$ orbital and is transformed into a second $^{HS}3d^8$ ion in [$Co^{I}Co^{I}$] (**B**). This is the proposed catalytically active species. The two adjacent $d_{x^2-y^2}$ SOMOs in **B** do not overlap spatially and, therefore, are not coupled with each other. As a consequence, each of these electrons can be transferred onto an incoming H^+ to reduce it to a hydride (H^-). As a result, protonation of **B** is favorable by 28 kcal mol^{-1} (ΔG). Each of the two $^{HS}Co^{I}$ centers transfers one electron from its $d_{x^2-y^2}$ SOMO, and the resulting complex is described as the species [$Co^{II}Co^{II}(H^-)$] (**C**) (Figure 8 and Figure S6 in the Supporting Information). The hydride moiety is bound more tightly to one of the Co^{II} ions, rather than symmetrically bridged between the two centers. The shortest Co^{II}–H^- distance is calculated at 1.54 Å, whereas the other distance has a computed value of 1.85 Å. It is noteworthy that the cooperativity between both centers in species **B** leads to **C**, [$Co^{II}Co^{II}(H^-)$], thereby precluding formation of a [$Co^{I}Co^{III}(H^-)$] intermediate. The latter species, containing the trivalent $3d^6$ Co^{III} ion, can only be invoked if there is no cooperativity and the two metal centers function independently. Succinctly, protonation of one of the Co^{I} centers in **B** prompts a 2 e^- transfer in which each of the two Co^{I} centers donates an electron to the H^+. As a result, the more reactive $Co^{II}(H^-)$ unit is achieved without prior or concurrent formation of the $Co^{III}(H^-)$ moiety.

Conclusion

We have investigated both experimentally and theoretically the bimetallic complex [$Co^{II}_2(L^1)(bpy)_2$]ClO_4 (**1**). This species supports the catalytic H^+ reduction to H_2 in CH_3CN in the presence of a weak acid such as HOAc at an overpotential of 0.63 V. This catalytic activity relies on a 2 e^- reduction of the parent species [$Co^{II}Co^{II}$] (**1**) to form a [$Co^{I}Co^{I}$] complex. Each of these Co^{I} centers contributes with the donation of one electron to a single incoming H^+, thus forming a reactive Co^{II}-hydride. The new bimetallic cooperativity exhibited by this system arises from the close proximity of the cobalt centers and an appropriate orbital topology that avoids the formation of the Co^{III}–H^- moiety required for proton reduction in monometallic catalysts. The second Co^{I} center plays a pivotal role in the catalytic reduction of H^+, acting as an electron reservoir to donate the second electron necessary for formation of the Co^{II}–H^- unit that favorably accepts another H^+ and releases H_2. Post-catalytic SEM and EDX analyses support the molecular nature of the catalyst. Therefore, the observations resulting from this work lead to considerations on how to optimize topology and orbital overlap to promote the use of a neighboring metal center as electron reservoir. These factors will become pivotal in the development of new and improved bimetallic catalysts.

Experimental Section

Materials and methods

Reagents were used without further purification as purchased from commercial sources. UV/Vis spectra were obtained using a Shimadzu UV-3600 spectrophotometer. Complex **1** was obtained by dissolving the ligand H_3L^1 (0.066 g, 0.10 mmol), 2,2′-bipyridine (bpy, 0.032 g, 0.20 mmol), and $Co(ClO_4)_2{\cdot}6H_2O$ (0.073 g, 0.2 mmol) in a 1:1 mixture of CH_3CN and CH_2Cl_2 (10 mL). A detailed synthetic protocol and characterizations have been described recently.[27]

Redox studies

The electrochemical behavior of **1** was investigated with a BAS 50W potentiostat/galvanostat. CVs were obtained at room temperature in CH_3CN containing 0.1 M $TBAPF_6$ as the supporting electrolyte under argon atmosphere. The electrochemical cell employed three electrodes: glassy-carbon (working), platinum wire (auxiliary), and Ag/AgCl (reference). The Fc^+/Fc redox couple [E^o = 401 mV vs. normal hydrogen electrode (NHE)] was used as internal standard. BE was performed in a custom-made air-tight H-type cell under inert conditions according to a procedure reported by Verani and co-workers.[24] The cell was comprised of two compartments separated by a frit. On one side of the frit were placed the Hg-pool working and Ag/AgCl reference electrodes, whereas a coiled 30.5 cm Pt wire serving as the auxiliary electrode was placed in the other compartment. BE experiments were performed in CH_3CN (20 mL) with $TBAPF_6$ as the supporting electrolyte until the calculated final charges were reached. All potentials were measured vs. Ag/AgCl. During BE, potentials were controlled with a BAS 50W potentiometer, and UV/Vis spectra were collected on a Shimadzu UV-3600 UV/Vis-NIR spectrophotometer at room temperature.

Computational studies

Electronic structure calculations were performed using the BPW91 density functional[37,38] as implemented in a development version of Gaussian.[39] The SDD basis set and effective core potential[40] were used for Co atoms, and the 6-31G(d,p) basis set[41,42] was used for the other atoms. To streamline calculations, a slightly modified model was used in which the *tert*-butyl substituents of complex **1** were replaced by methyl groups. Geometry optimization was performed in the gas phase, and all optimized structures were confirmed as minima by harmonic vibrational frequency calculations. The energies of the optimized structures were reevaluated by additional single-point calculations on each optimized geometry in CH_3CN by using the implicit SMD solvation model.[43] The converged wave functions in solvent were tested for self-consistent field (SCF) stability. The free energy in solution phase G(sol) was calculated as follows: $G(sol) = E_{SCF}(sol) + [\text{zero-point energy(ZPE)} + \text{thermal correction} - TS](gas)$. E_{SCF} was calculated in the solvent, whereas ZPE, thermal correction, and entropic contributions were calculated in the gas phase. The standard states of 1 M concentration were considered for all reactants and products for calculating the free energies of reactions [ΔG(sol)]. The spin-density plots (isovalue = 0.004 a.u.) and corresponding orbitals[44] (isovalue = 0.05 a.u.) of the calculated structures were visualized with GaussView.[45] The literature value[46] of −264.6 kcal mol^{-1} was used for the free energy of a proton in CH_3CN. The calculation of the reduction potentials (E, V in Volt) of the complexes included ZPE, thermal correction, and entropic contribution. The standard thermodynamic equation $\Delta G(sol) = -nFE$ was used. The calculated potentials were referenced to a value of $E_{1/2}$ = 4.38 V for the Fc^+/Fc couple calculated under our level of theory.

Catalytic studies

Electrocatalytic studies to determine the amount of H produced by the catalyst, TONs, and FEs were performed as previously de-

scribed[24] in an H-type cell (Hg-pool; Ag/AgCl | Pt-coil). The main chamber was filled with catalyst **1** (0.005 g, 4×10^{-6} mol), and the $TBAPF_6$ electrolyte (1.56 g) and acetic acid (0.024 g, 4×10^{-4} mol, 100 equiv) were dissolved in CH_3CN (20 mL). The small chamber housing the auxiliary electrode was filled with $TBAPF_6$ (0.390 g) in CH_3CN (5 mL). In a typical test, the cell was purged for 20 min followed by sampling the head space gas with a Gow-Mac 400 GC equipped with a thermal conductivity detector and a 2.4 m × 0.31 cm × 5 Å molecular-sieve column operating at a temperature of 60 °C. The amount of H_2 produced was determined by GC with a calibration curve obtained with known volumes of 99.999 + % H_2 gas and shown in Figure S1 in the Supporting Information (see the Supporting Information for sample data and relevant calculations obtained from experiments). A catalyst-free solution was electrolyzed for 3 h and analyzed by GC to provide a blank. The cell was then purged again, and the catalyst was added. Electrolysis ensued for 3 h, and the headspace with H_2 gas was analyzed. The TON was then calculated after background subtraction as the ratio between mol H_2 produced per mol catalyst. The FE was calculated from the GC measurements.

Acknowledgements

This research was made possible by the Division of Chemical Sciences, Geosciences, and Biosciences, Office of Basic Energy Sciences of the U.S. Department of Energy through the Single-Investigator and Small-Group Research (SISGR)–Solar Energy program grants DE-SC0001907 and DE-FG02-09ER16120 to C.N.V. and H.B.S., including financial support to K.K.K. and S.M. A.T.F. acknowledges support from the NSF (CHE-1056845). K.K.K. also acknowledges WSU-Chemistry for a Thomas C. Rumble Graduate Fellowship.

Conflict of interest

The authors declare no conflict of interest.

Keywords: bimetallic complexes · bimetallic cooperativity · cobalt · Co^{II}–H^- species · proton reduction

[1] J. A. Turner, *Science* **2004**, *305*, 972 – 974.
[2] N. S. Lewis, D. G. Nocera, *Proc. Natl. Acad. Sci. USA* **2006**, *103*, 15729 – 15735.
[3] A. D. Wilson, R. H. Newell, M. J. McNevin, J. T. Muckerman, M. Rakowski DuBois, D. L. DuBois, *J. Am. Chem. Soc.* **2006**, *128*, 358 – 366.
[4] P. A. Jacques, V. Artero, J. Pecaut, M. Fontecave, *Proc. Natl. Acad. Sci. USA* **2009**, *106*, 20627 – 20632.
[5] L. Chen, M. Wang, F. Gloaguen, D. Zheng, P. Zhang, L. Sun, *Inorg. Chem.* **2013**, *52*, 1798 – 1806.
[6] P. H. A. Kankanamalage, S. Mazumder, V. Tiwari, K. K. Kpogo, H. Bernhard Schlegel, C. N. Verani, *Chem. Commun.* **2016**, *52*, 13357 – 13360.
[7] P. Connolly, J. H. Espenson, *Inorg. Chem.* **1986**, *25*, 2684 – 2688.
[8] B. H. Solis, S. Hammes-Schiffer, *J. Am. Chem. Soc.* **2011**, *133*, 19036 – 19039.
[9] B. H. Solis, S. Hammes-Schiffer, *Inorg. Chem.* **2011**, *50*, 11252 – 11262.
[10] J. T. Muckerman, E. Fujita, *Chem. Commun.* **2011**, *47*, 12456 – 12458.
[11] B. H. Solis, Y. Yu, S. Hammes-Schiffer, *Inorg. Chem.* **2013**, *52*, 6994 – 6999.
[12] X. Hu, B. S. Brunschwig, J. C. Peters, *J. Am. Chem. Soc.* **2007**, *129*, 8988 – 8998.
[13] S. C. Marinescu, J. R. Winkler, H. B. Gray, *Proc. Natl. Acad. Sci. USA* **2012**, *109*, 15127 – 15131.
[14] E. S. Wiedner, R. M. Bullock, *J. Am. Chem. Soc.* **2016**, *138*, 8309 – 8318.
[15] E. S. Rountree, D. J. Martin, B. D. McCarthy, J. L. Dempsey, *ACS Catal.* **2016**, *6*, 3326 – 3335.
[16] S. Mandal, S. Shikano, Y. Yamada, Y. M. Lee, W. Nam, A. Llobet, S. Fukuzumi, *J. Am. Chem. Soc.* **2013**, *135*, 15294 – 15297.
[17] N. K. Szymczak, L. A. Berben, J. C. Peters, *Chem. Commun.* **2009**, 6729 – 6731.
[18] S. Kal, A. S. Filatov, P. H. Dinolfo, *Inorg. Chem.* **2014**, *53*, 7137 – 7145.
[19] a) N. H. Pilkington, R. Robson, *Aust. J. Chem.* **1970**, *23*, 2225 – 2236;
b) H. Ôkawa, H. Furutachi, D. E. Fenton, *Coord. Chem. Rev.* **1998**, *174*, 51 – 75.
[20] C. N. Valdez, J. L. Dempsey, B. S. Brunschwig, J. R. Winkler, H. B. Gray, *Proc. Natl. Acad. Sci. USA* **2012**, *109*, 15589 – 15593.
[21] S. M. Laga, J. D. Blakemore, L. M. Henling, B. S. Brunschwig, H. B. Gray, *Inorg. Chem.* **2014**, *53*, 12668 – 12670.
[22] C. Di Giovanni, C. Gimbert-Suriñach, M. Nippe, J. Benet-Buchholz, J. R. Long, X. Sala, A. Llobet, *Chem. Eur. J.* **2016**, *22*, 361 – 369.
[23] D. Basu, M. M. Allard, F. R. Xavier, M. J. Heeg, H. B. Schlegel, C. N. Verani, *Dalton Trans.* **2015**, *44*, 3454 – 3466.
[24] D. Basu, S. Mazumder, X. Shi, H. Baydoun, J. Niklas, O. Poluektov, H. B. Schlegel, C. N. Verani, *Angew. Chem. Int. Ed.* **2015**, *54*, 2105 – 2110; *Angew. Chem.* **2015**, *127*, 2133 – 2138.
[25] D. Basu, S. Mazumder, X. Shi, R. J. Staples, H. B. Schlegel, C. N. Verani, *Angew. Chem. Int. Ed.* **2015**, *54*, 7139 – 7143; *Angew. Chem.* **2015**, *127*, 7245 – 7249.
[26] D. Basu, S. Mazumder, J. Niklas, H. Baydoun, D. Wanniarachchi, X. Shi, R. J. Staples, O. Poluektov, H. B. Schlegel, C. N. Verani, *Chem. Sci.* **2016**, *7*, 3264 – 3278.
[27] D. Wang, S. V. Lindeman, A. T. Fiedler, *Inorg. Chem.* **2015**, *54*, 8744 – 8754.
[28] D. J. Martin, B. D. McCarthy, C. L. Donley, J. L. Dempsey, *Chem. Commun.* **2015**, *51*, 5290 – 5293.
[29] J. A. S. Roberts, R. M. Bullock, *Inorg. Chem.* **2013**, *52*, 3823 – 3835.
[30] V. Fourmond, P. A. Jacques, M. Fontecave, V. Artero, *Inorg. Chem.* **2010**, *49*, 10338 – 10347.
[31] J.-L. Calais, *Int. J. Quantum Chem.* **1993**, *47*, 101 – 101.
[32] S. Varma, C. E. Castillo, T. Stoll, J. Fortage, A. G. Blackman, F. Molton, A. Deronzier, M.-N. Collomb, *Phys. Chem. Chem. Phys.* **2013**, *15*, 17544 – 17552.
[33] B. de Bruin, E. Bill, E. Bothe, T. Weyhermüller, K. Wieghardt, *Inorg. Chem.* **2000**, *39*, 2936 – 2947.
[34] P. Tong, W. Xie, D. Yang, B. Wang, X. Ji, J. Li, J. Qu, *Dalton Trans.* **2016**, *45*, 18559—18565.
[35] When referenced to the experimental acid, acetic acid ($pK_a = 22.3$), protonation of Co^I–Co^I **B** will be slightly uphill by 2.6 kcal mol^{-1}. Similarly, protonation and release of H_2 from **C** will be downhill by 19.2 kcal mol^{-1}.
[36] J. K. Hurst, M. D. Roemeling, S. V. Lymar, *J. Phys. Chem. B* **2015**, *119*, 7749 – 7760.
[37] A. D. Becke, *Phys. Rev. A* **1988**, *38*, 3098 – 3100.
[38] J. P. Perdew, Y. Wang, *Phys. Rev. B* **1992**, *45*, 13244 – 13249.
[39] Gaussian Development Version, Revision H.31, M. J. Frisch, G. W. Trucks, H. B. Schlegel, G. E. Scuseria, M. A. Robb, J. R. Cheeseman, G. Scalmani, V. Barone, B. Mennucci, G. A. Petersson, H. Nakatsuji, M. Caricato, X. Li, H. P. Hratchian, A. F. Izmaylov, J. Bloino, G. Zheng, J. L. Sonnenberg, W. Liang, M. Hada, M. Ehara, K. Toyota, R. Fukuda, J. Hasegawa, M. Ishida, T. Nakajima, Y. Honda, O. Kitao, H. Nakai, T. Vreven, J. A. Montgomery, Jr., J. E. Peralta, F. Ogliaro, M. Bearpark, J. J. Heyd, E. Brothers, K. N. Kudin, V. N. Staroverov, T. Keith, R. Kobayashi, J. Normand, K. Raghavachari, A. Rendell, J. C. Burant, S. S. Iyengar, J. Tomasi, M. Cossi, N. Rega, J. M. Millam, M. Klene, J. E. Knox, J. B. Cross, V. Bakken, C. Adamo, J. Jaramillo, R. Gomperts, R. E. Stratmann, O. Yazyev, A. J. Austin, R. Cammi, C. Pomelli, J. W. Ochterski, R. L. Martin, K. Morokuma, V. G. Zakrzewski, G. A. Voth, P. Salvador, J. J. Dannenberg, S. Dapprich, P. V. Parandekar, N. J. Mayhall, A. D. Daniels, O. Farkas, J. B. Foresman, J. V. Ortiz, J. Cioslowski, D. J. Fox, Gaussian, Inc., Wallingford CT, **2010**.
[40] M. Dolg, U. Wedig, H. Stoll. H. Preuss, *J. Chem. Phys.* **1987**, *86*, 866 – 872.
[41] P. C. Hariharan, J. A. Pople, *Theor. Chim. Acta* **1973**, *28*, 213 – 222.

[42] M. M. Francl, W. J. Pietro, W. J. Hehre, J. S. Binkley, M. S. Gordon, D. J. DeFrees, J. A. Pople, *J. Chem. Phys.* **1982**, *77*, 3654-3665.
[43] A. V. Marenich, C. J. Cramer, D. G. Truhlar, *J. Phys. Chem. B* **2009**, *113*, 6378 – 6396.
[44] F. Neese, *Phys. Chem. Solids* **2004**, *65*, 781 – 785.
[45] R. D. Dennington II, T. A. Keith, J. M. Millam, GaussView, Version 5, Semichem Inc., Shawnee Mission, KS, **2009**.
[46] C. P. Kelly, C. J. Cramer, D. G. Truhlar, *J. Phys. Chem. A* **2006**, *110*, 16066 – 16081.

Manuscript received: May 3, 2017
Accepted manuscript online: May 9, 2017
Version of record online: June 23, 2017